VIP Charge Transfer

DOI: 10.1002/ange.201000171

Comparing Spin-Selective Charge Transport through Donor–Bridge–Acceptor Molecules with Different Oligomeric Aromatic Bridges**

*Amy M. Scott, Annie Butler Ricks, Michael T. Colvin, and Michael R. Wasielewski**

The design of molecular systems for solar energy conversion that are capable of moving charge efficiently over long distances through molecular bridges requires a fundamental understanding of electron transport in donor–bridge–acceptor (D-B-A) systems. Charge transport has been studied in covalently linked D-B-A systems with various bridge molecules, including proteins,[1] DNA,[2] porphyrins,[3] and saturated[4] and unsaturated hydrocarbons.[5] Nevertheless, in many of these systems, multiple charge-transport mechanisms and pathways exist and the factors that favor particular mechanisms remain poorly understood. Continuing efforts toward understanding how the electronic structure and composition of the bridge governs the charge transport mechanism, and thus the lifetimes of photogenerated radical ion pairs (RPs), are important for the rational design of "molecular wires".[6]

Bridge-mediated charge transport by the superexchange mechanism involves mixing of bridge states with those of the donor and acceptor and requires the bridge states to be energetically higher than and well-separated from those of the donor, thus resulting in an exponential dependence of the charge transport rate constant on distance [Eq. (1)],

$$k = k_0 e^{-\beta(r-r_0)} \quad (1)$$

where k_0 is the rate constant at the van der Waals contact distance r_0 (3.5 Å), and β is the damping coefficient for the decay. For systems that undergo superexchange charge transport, the overall electronic coupling matrix element V_{DA} for charge transport is inversely dependent on the energy gap between the donor and bridge states, as described by McConnell[6d] [Eq. (2)],

$$V_{DA} = \frac{V_{DB}V_{BA}}{\Delta E_{DB}}\left(\frac{V_{BB}}{\Delta E_{DB}}\right)^{N-1} \quad (2)$$

where V_{DB} and V_{BA} are the matrix elements that couple the donor to the bridge and the bridge to the acceptor, respectively, V_{BB} is the electronic coupling between bridge sites, N is the number of identical bridge sites, and ΔE_{DB} is the energy gap for charge injection from the donor to the virtual bridge state.[6d,7]

If the bridge states are comparable in energy to those of the donor, direct oxidation or reduction of the bridge may result in a charge hopping mechanism that has a much weaker distance dependence than a superexchange mechanism. The use of rigid donors and acceptors with varying bridge lengths allows for the measurement of distance-dependent charge-transfer rates to elucidate how the superexchange and hopping charge-transfer regimes within molecular systems depend on structure.[2a,8] However, even in molecules that have well-defined D-B-A distances, internal degrees of freedom, such as single-bond torsions, often modulate the magnitude of V_{DA}. Moreover, earlier work on oligomeric π-conjugated bridges, such as *p*-phenylenevinylene,[9] *p*-phenylene,[10] and fluorene[6b] has demonstrated that a switch in mechanism from superexchange to hopping can occur at longer bridge lengths.

Herein, we describe a systematic study of charge-recombination (CR) distance dependence for photogenerated RPs in a series of covalent D-B-A systems. The subunits are linked by conjugated molecular bridges that consist of fluorenone ($n = 1$–3) (FN_n) and *p*-phenylethynylene ($n = 1$–3) (PE_nP) covalently attached to a 3,5-dimethyl-4-(9-anthracenyl) julolidine (DMJ-An) electron donor and a naphthalene-1,8:4,5-bis(dicarboximide) (NI) electron acceptor. The CR rates, measured by nanosecond transient absorption spectroscopy, are compared to those of a previously published system,[11] in which *p*-phenylene bridges (Ph_n) ($n = 1$–5) are appended to the same DMJ-An donor and NI acceptor (Figure 1a). Photoexcitation of these systems results in rapid formation of a singlet RP, which undergoes electron–nuclear hyperfine coupling-induced radical pair intersystem crossing (RP-ISC) to produce the triplet RP, that is, $^1(D^{+\bullet}\text{-B-}A^{-\bullet}) \rightarrow {}^3(D^{+\bullet}\text{-B-}A^{-\bullet})$. Subsequent CR is spin selective; that is, the singlet RP recombines to the singlet ground state and the triplet RP recombines to yield the neutral local triplet (Figure 1b). By monitoring the yield of local triplet production as a function of applied magnetic field B, the magnitude of the spin–spin exchange interaction $2J$ can be measured directly,[12] and can be used to estimate V_{DA} because $2J \propto V_{DA}^2$.[10,13] Magnetic field effects (MFEs) and time-resolved EPR (TREPR) spectroscopy were used to measure the $2J$ value, and a kinetic analysis of the MFE data was used to separate the rate constants for the spin-selective CR pathways.

[*] Dr. A. M. Scott, A. Butler Ricks, M. T. Colvin, Prof. M. R. Wasielewski
Department of Chemistry and
Argonne Northwestern Solar Energy Research Center (ANSER)
Northwestern University
2145 Sheridan Road, Evanston, IL 60208 (USA)
Fax: (+1) 847-467-1425
E-mail: m-wasielewski@northwestern.edu

[**] We thank Dr. Tomoaki Miura for helpful discussions. This work is supported by the Chemical Sciences, Geosciences, and Biosciences Division, Office of Basic Energy Sciences, DOE under grant no. DE-FG02-99ER14999.

Supporting information (detailed information on sample preparation, transient absorption spectroscopy, TREPR spectroscopy, and kinetic analyses) for this article is available on the WWW under http://dx.doi.org/10.1002/anie.201000171.

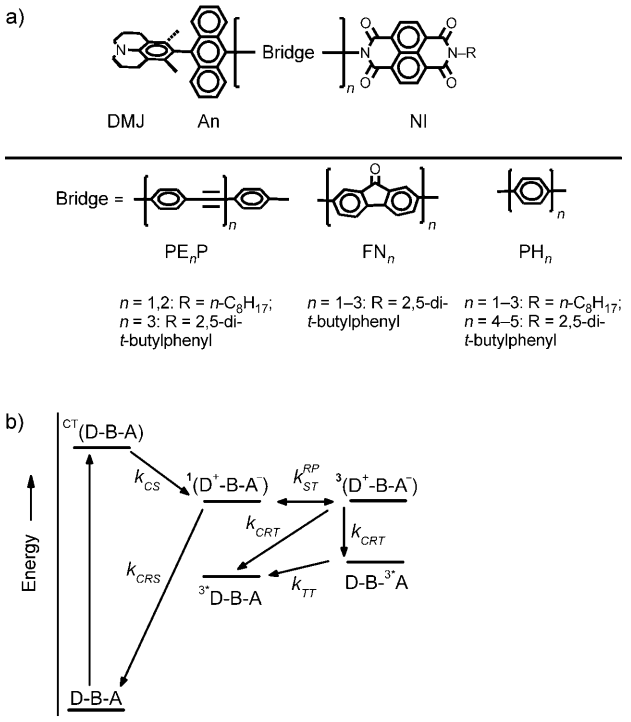

Figure 1. a) Donor–bridge–acceptor systems used in this study. b) Charge transfer scheme for FN_{1-3}, $PE_{1-3}P$, and Ph_{1-5}.

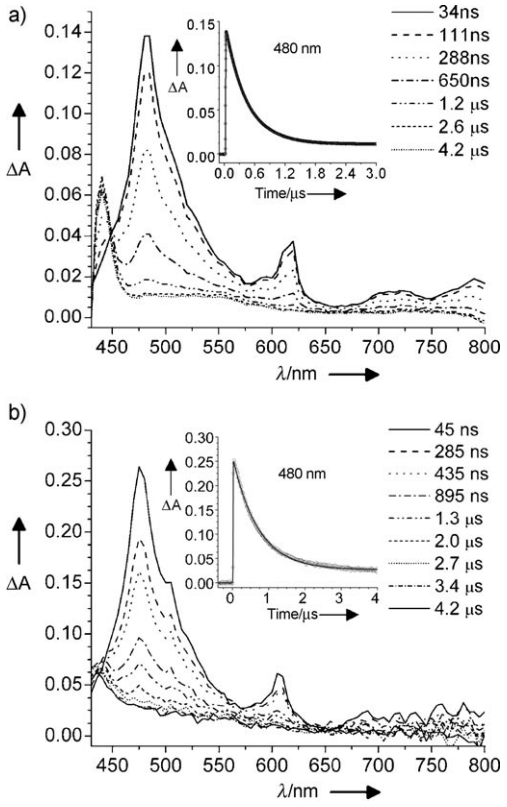

Figure 2. a) Transient absorption spectra of FN_2 in toluene at 295 K at the indicated times following a 7 ns, 416 nm laser pulse. Inset: transient absorption kinetics at 480 nm. b) Transient absorption spectra of PE_2P in toluene at 295 K at the indicated times following a 7 ns, 416 nm laser pulse. Inset: transient absorption kinetics at 480 nm. Data points obtained every 5 nm.

The ground-state absorption spectrum of DMJ-An in toluene exhibits a broad charge-transfer (CT) absorption maximum at 367 nm with a broad emission maximum at 519 nm, which result in an excited singlet CT state energy in toluene of 2.89 eV.[14] The absorption spectra of DMJ-An-FN$_n$-NI and DMJ-An-PE$_n$P-NI for $n=1$–3 are shown in Figure S1 in the Supporting Information. Femtosecond transient absorption spectroscopy was used to determine the charge separation (CS) rate constants, k_{CS} (Table S1 in the Supporting Information). Selective photoexcitation of the DMJ-An CT band in DMJ-An-FN$_n$-NI and DMJ-An-PE$_n$P-NI in toluene for $n=1$–3 with 416 nm, 110 fs laser pulses results in nearly quantitative CS to give DMJ$^{+\bullet}$-An$^{-\bullet}$ followed by a rapid charge shift to yield DMJ$^{+\bullet}$-An-FN$_n$-NI$^{-\bullet}$ and DMJ$^{+\bullet}$-An-PE$_n$P-NI$^{-\bullet}$, respectively.

Nanosecond transient absorption spectroscopy was used to determine the subsequent CR rate constants k_{CR} by measuring the lifetimes of the prominent NI$^{-\bullet}$ features at 480 nm and 610 nm following excitation with 416 nm, 7 ns laser pulses. Data for the FN_2 and PE_2P bridges are shown in Figure 2a,b. Following rapid CS, the initially formed singlet RPs, ^{1}(DMJ$^{+\bullet}$-An-FN$_n$-NI$^{-\bullet}$) and ^{1}(DMJ$^{+\bullet}$-An-PE$_n$P-NI$^{-\bullet}$), undergo rapid RP-ISC to produce the respective triplet RPs, ^{3}(DMJ$^{+\bullet}$-An-FN$_n$-NI$^{-\bullet}$) and ^{3}(DMJ$^{+\bullet}$-An-PE$_n$P-NI$^{-\bullet}$). The energy levels of these triplet RP states are above those of ^{3}*An and ^{3}*NI, so that spin-selective CR can occur from the triplet RPs to produce (DMJ-An-FN$_n$-^{3}*NI) and (DMJ-An-PE$_n$P-^{3}*NI) ($E_T=2.03$ eV),[15] as well as (DMJ-^{3}*An-FN$_n$-NI) and (DMJ-^{3}*An-PE$_n$P-NI), respectively ($E_T=1.85$ eV).[16] For spin-selective CR to ^{3}*NI and ^{3}*An, the broad absorption features at 480 nm and 430 nm[17] persist on the microsecond timescale and appear as plateaus in the kinetic traces (Figure 2, insets). The decay-associated spectra for the FN_2 and PE_2P bridges indicate that CR to both ^{3}*An and ^{3}*NI is limited by the lifetimes of their RPs (Figure S2 in the Supporting Information). The lifetimes obtained by fitting individual kinetic traces match those of the decay-associated spectra.

MFEs were used to measure the magnitude of $2J$ in the RPs by quantifying the triplet yield, radical pair yield, and CR rate as a function of B for the FN$_n$ and PE$_n$P bridges in toluene at 295 K. Application of a magnetic field results in Zeeman splitting of the triplet RP energy levels, which are labeled T_{+1}, T_0, and T_{-1} at fields that are high relative to the sum of the hyperfine couplings within the RP (Figure S3 in the Supporting Information). The maximum of the relative triplet yield plot and the minimum of the relative RP yield plot occur at $B=2J$, the field at which the S and T_{+1} (if $2J>0$) or T_{-1} (if $2J<0$) RP energy levels cross, and the magnitude of $2J$ is directly proportional to V_{DA}.[10] The results show that the $2J$ value for the FN_1 bridge (40 mT) is larger than that for PE_1P (13.5 mT) (Figure 3a,b). Interestingly, the $2J$ values for FN_2 and PE_2P are both 3 mT (Figure S4 in the Supporting Information), which is explained by evaluating the exponential distance dependence of $2J$, where $2J=2J_0e^{-\alpha(r-r_0)}$.[10,13] The RP distances for DMJ$^{+\bullet}$-An-FN$_2$-NI$^{-\bullet}$ and DMJ$^{+\bullet}$-An-

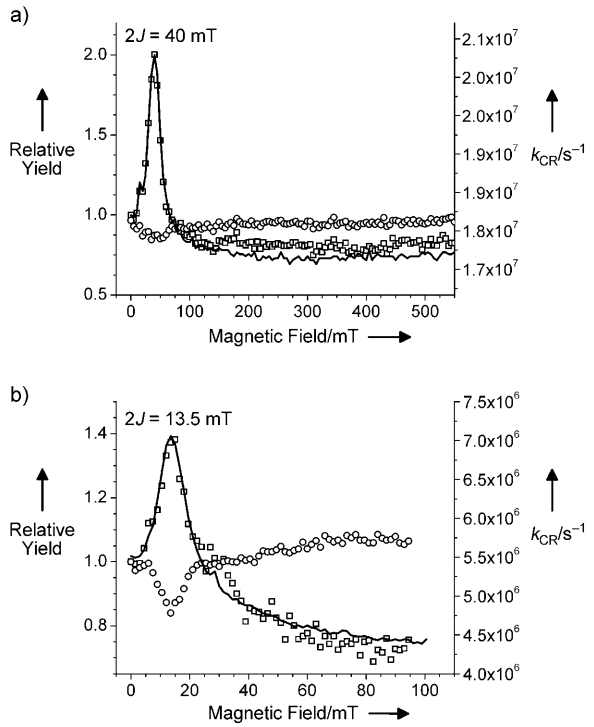

Figure 3. Relative triplet yield (□), radical pair yield (○), and CR rate (——) versus magnetic field for a) FN_1 in toluene at 480 nm at 87 ns (RP) after the laser flash and b) PE_1P in toluene at 480 nm at 114 ns (RP) after the laser flash.

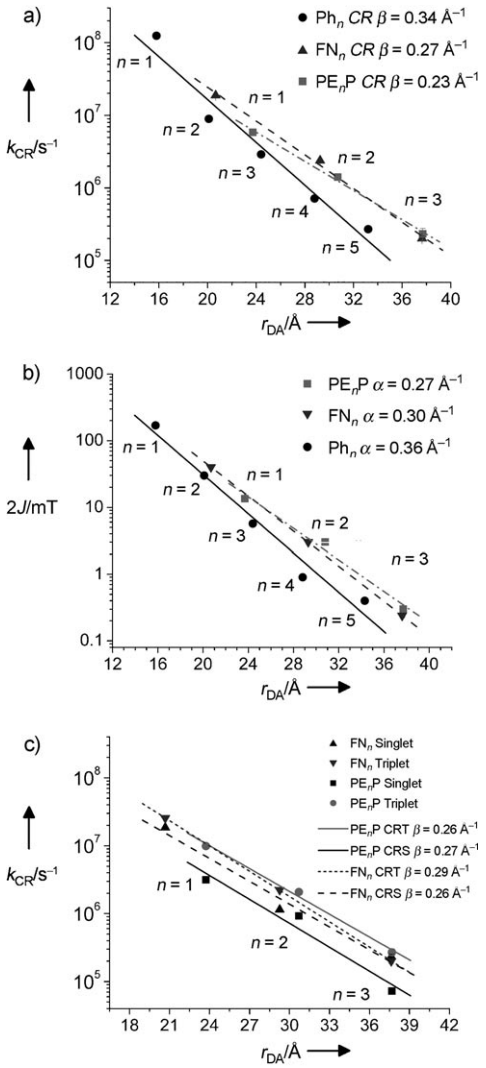

Figure 4. a) Plots of k_{CR} for PE_nP ($R^2 = 0.995$), k_{CR} for FN_n ($R^2 = 0.997$), and k_{CR} for Ph_n ($R^2 = 0.960$), versus r_{DA} distance (at 295 K). The lines show the linear fits. b) Logarithmic plot of the spin–spin exchange interaction 2*J* versus distance r_{DA}. c) Plot of k_{CRT} and k_{CRS} versus r_{DA}. The error bars on the data points are smaller than the size of the symbols for all plots.

PE_2P-$NI^{-\bullet}$ estimated from B3LYP/STO-3G calculations are both approximately 30 Å (Tables S2 and S3 in the Supporting Information). A similar situation prevails for the PE_3P and FN_3 bridges, which both have RP distances of 37 Å and the 2*J* value is determined by fitting the TREPR spectra of the radical pairs (Figure S5 in the Supporting Information). These data, together with an examination of the rate versus magnetic field plots (Figure 3 and Figure S4 in the Supporting Information) indicate that the triplet CR pathway is more efficient for the $FN_{1\text{-}3}$ and $PE_{1\text{-}3}P$ bridges, as was also observed earlier for the $Ph_{2\text{-}5}$ bridges,[11] because the CR rate increases as the triplet yield increases at the 2*J* resonance.

A semi-log plot of the observed rate k_{CR} versus distance for Ph_n, PE_nP, and FN_n at 295 K in toluene (Figure 4a) shows that k_{CR} depends exponentially on distance and that a superexchange mechanism dominates the CR process with $\beta = 0.34$ Å^{-1}, 0.23 Å^{-1}, and 0.27 Å^{-1}, respectively. Since the redox potentials for most conjugated bridge molecules, including *p*-phenylene,[18] *p*-phenylethynylene,[19] and fluorenone, vary with bridge length, the charge injection energy gap is also distance-dependent. As the bridge length increases, the energy gap may become sufficiently small so that oxidation or reduction of the bridge is allowed and crossover from a superexchange to a charge-hopping mechanism may occur. Our estimation of the RP energies with increasing bridge length indicates that a hopping mechanism cannot occur for CR in these series of molecules with Ph_n, FN_n, and PE_nP bridges (Tables S2, S3 and Figure S6 in the Supporting Information). This hypothesis is further supported by analyzing the distance dependence of 2*J* because this dependence directly monitors the decay of the superexchange interaction.[10] The plot of 2*J* versus distance (Figure 4b) yields an exponential distance decay parameter α of 0.36 Å^{-1} for Ph_n, 0.27 Å^{-1} for PE_nP, and 0.30 Å^{-1} for FN_n. These data show that the value of V_{DA} increases in the order $PE_nP > FN_n > Ph_n$.

We have analyzed the distance dependence of the experimentally observed CR rate k_{CR} but the spin-selective CR pathways, k_{CRS} and k_{CRT}, must also be examined to understand how charge transport mechanisms depend on spin dynamics. A kinetic analysis of the MFE data has been described previously that can yield rates for the singlet and triplet CR pathways.[11] Briefly, the model assumes that the initial population resides on the singlet RP (S in Figure 5), and depending on the magnitude of 2*J* (i.e., the S–T_0 gap), RP-ISC to the triplet RP (T in Figure 5) occurs through

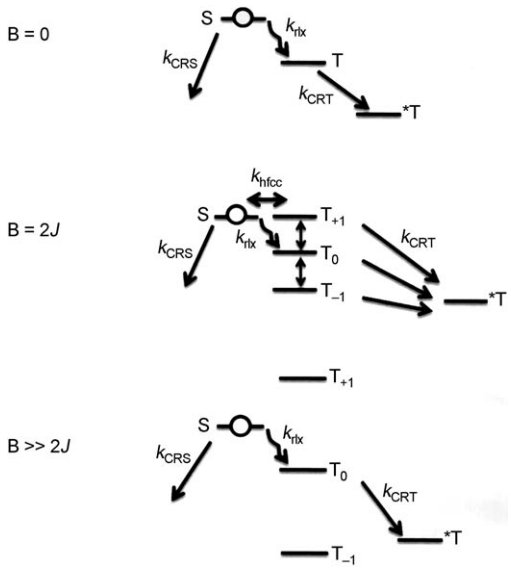

Figure 5. Kinetic model used to separate k_{CRS} and k_{CRT} pathways for FN_1 and PE_1P. MFE kinetics are analyzed under three conditions: $B=0$, $B=2J$, and $B \gg 2J$. T_{+1}, T_0, and T_{-1} correspond to the triplet RP sublevels that split by the Zeeman interaction at magnetic field B. T* denotes the lowest excited triplet state whose energy is far below that of the RP energy levels. The circle indicates that the singlet RP is initially populated.

hyperfine (k_{hfcc}) and spin relaxation (k_{rlx}) mechanisms. The kinetic equations can be solved analytically or numerically using k_{obs}. In the latter case, the kinetic equations for $B=0$, $B=2J$, and $B \gg 2J$ are simulated using the kinetic model (described in Figure S7 in the Supporting Information).

For FN_1, the analytical expression gives nearly identical results to the numerical fit of the kinetic data. The kinetics at $B=0$ and $B \gg 2J$ are virtually the same, with negligible triplet yields. S–T_0 relaxation is much slower than the RP lifetime because $2J$ is large (40 mT) and the RP lifetime is short (54 ns). Although the triplet CR pathway is more efficient, intersystem crossing between the singlet and triplet RP states is slow (261 ns), and the singlet channel dominates the population flow. Numerical fitting was only used for PE_1P since the $2J$ value (13.5 mT) is greater than a_{hfcc}, where a_{hfcc} is the hyperfine interaction. For $FN_{2\text{-}3}$ and $PE_{2\text{-}3}P$, $2J \leq a_{hfcc}$, so that RP-ISC can be explained by the conventional hyperfine and relaxation mechanisms.[20] Briefly, the kinetics are solved analytically with the apparent decay described at $B=0$ by $k_{obs}=0.25\,k_{CRS}+0.75\,k_{CRT}$ and at $B \gg 2J$ by $k_{obs}=0.5\,k_{CRS}+0.5\,k_{CRT}$, which are governed by spin statistics (see Table S1 in the Supporting Information).

The distance dependencies of k_{CRS} and k_{CRT} for the FN_n and PE_nP bridges, where k_{CRT} denotes the total CR rate to both ^{3}*An and ^{3}*NI, are shown in Figure 4c. An explanation of the data requires an examination of the interplay of the electronic coupling V_{BB}, the energy gap between the donor and bridge ΔE_{DB}, and the RP distance r, which are all reflected in β for a superexchange process [Eq. (3)]:

$$\beta = \frac{2}{r}\ln\left(\frac{\Delta E_{DB}}{V_{BB}}\right) \qquad (3)$$

For spin-selective CR, the triplet pathway is more efficient for the $FN_{1\text{-}3}$ and $PE_{1\text{-}3}P$ bridges, as is also the case for the longer bridge lengths in the Ph_n series. This observation is corroborated by the MFE results (Figure 3) and can be understood by considering the energy gap dependence for the two CR pathways, where $^3[D^{+\bullet}\text{-}B\text{-}A^{-\bullet}] \rightarrow [D\text{-}B\text{-}^3A]$ and $[^3*D\text{-}B\text{-}A]$ are both in the Marcus normal region ($|\Delta G| < 0.50$ eV) and $^1[D^{+\bullet}\text{-}B\text{-}A^{-\bullet}] \rightarrow D\text{-}B\text{-}A$ is in the inverted region ($|\Delta G| > 2.0$ eV).[21] The β values for the FN_n and PE_nP bridges, and their singlet and triplet CR pathways, are comparable in magnitude. This result may seem surprising compared to our earlier results for Ph_n, which reveal that β is larger for singlet CR than triplet CR, but is a consequence of coincidental balancing of the effects of ΔE_{DB} and V_{BB} in Equation (3). The predicted LUMO energies (Figure S8 in the Supporting Information) for these bridges illustrate that ΔE_{DB} for Ph_n is greater than that for PE_nP and FN_n, in the order $Ph_n > PE_nP > FN_n$. The relationships between these parameters highlight the fact that β for both singlet and triplet charge recombination is system-dependent, not bridge-specific.

We have investigated photoinduced charge transport in a series of D-B-A molecules that have the same donor and acceptor but different oligomeric conjugated bridges, in order to understand how the charge-transport mechanism depends on molecular structure. We have demonstrated that the distance dependence of the spin-selective CR pathways can be separated by a kinetic analysis of the MFE data, and that those pathways in the FN_n and PE_nP bridges have coincidentally similar β values. Experiments that examine the temperature dependence on k_{CR} are currently in progress. These experiments will help elucidate the role of bridge dynamics, especially torsional motions, in the charge transport process. In the pursuit of organic materials for solar energy conversion, a detailed understanding of the charge transport pathways is critical for designing systems for both solar fuels and electricity production.

Received: January 12, 2010
Published online: March 15, 2010

Keywords: conjugation · donor–acceptor systems · electron transfer · energy conversion · intersystem crossing

[1] H. B. Gray, J. R. Winkler, *Proc. Natl. Acad. Sci. USA* **2005**, *102*, 3534.
[2] a) J. Jortner, M. Bixon, T. Langenbacher, M. E. Michel-Beyerle, *Proc. Natl. Acad. Sci. USA* **1998**, *95*, 12759; b) P. Daublain, K. Siegmund, M. Hariharan, J. Vura-Weis, M. R. Wasielewski, F. D. Lewis, V. Shafirovich, Q. Wang, M. Raytchev, T. Fiebig, *Photochem. Photobiol. Sci.* **2008**, *7*, 1501.
[3] Y. Kobori, S. Yamauchi, K. Akiyama, S. Tero-Kubota, H. Imahori, S. Fukuzumi, J. R. Norris, Jr., *Proc. Natl. Acad. Sci. USA* **2005**, *102*, 10017.
[4] B. P. Paulson, J. R. Miller, W. X. Gan, G. Closs, *J. Am. Chem. Soc.* **2005**, *127*, 4860.
[5] a) B. Albinsson, J. Martensson, *J. Photochem. Photobiol. C* **2008**, *9*, 138; b) M. Wielopolski, C. Atienza, T. Clark, D. M. Guldi, N. Martin, *Chem. Eur. J.* **2008**, *14*, 6379.
[6] a) B. Albinsson, M. P. Eng, K. Pettersson, M. U. Winters, *Phys. Chem. Chem. Phys.* **2007**, *9*, 5847; b) R. H. Goldsmith, L. E.

Sinks, R. F. Kelley, L. J. Betzen, W. H. Liu, E. A. Weiss, M. A. Ratner, M. R. Wasielewski, *Proc. Natl. Acad. Sci. USA* **2005**, *102*, 3540; c) M. Bixon, J. Jortner, *J. Chem. Phys.* **1997**, *107*, 5154; d) H. M. McConnell, *J. Chem. Phys.* **1961**, *35*, 508; e) M. N. Paddon-Row, A. M. Oliver, J. M. Warman, K. J. Smit, M. P. de Haas, H. Oevering, J. W. Verhoeven, *J. Phys. Chem.* **1988**, *92*, 6958.

[7] M. A. Ratner, *J. Phys. Chem.* **1990**, *94*, 4877.

[8] a) C. Lambert, G. Noll, J. Schelter, *Nat. Mater.* **2002**, *1*, 69; b) W. B. Davis, M. R. Wasielewski, M. A. Ratner, V. Mujica, A. Nitzan, *J. Phys. Chem. A* **1997**, *101*, 6158; c) M. D. Johnson, J. R. Miller, N. S. Green, G. L. Closs, *J. Phys. Chem.* **1989**, *93*, 1173; d) M. Bixon, J. Jortner, *Adv. Chem. Phys.* **1999**, *106*, 3.

[9] W. B. Davis, W. A. Svec, M. A. Ratner, M. R. Wasielewski, *Nature* **1998**, *396*, 60.

[10] E. A. Weiss, M. J. Ahrens, L. E. Sinks, A. V. Gusev, M. A. Ratner, M. R. Wasielewski, *J. Am. Chem. Soc.* **2004**, *126*, 5577.

[11] A. M. Scott, T. Miura, A. B. Ricks, Z. E. X. Dance, E. M. Giacobbe, M. T. Colvin, M. R. Wasielewski, *J. Am. Chem. Soc.* **2009**, *131*, 17655.

[12] a) P. W. Anderson, *Phys. Rev.* **1959**, *115*, 2; b) D. A. Shultz, R. M. Fico, Jr., S. H. Bodnar, R. K. Kumar, K. E. Vostrikova, J. W. Kampf, P. D. Boyle, *J. Am. Chem. Soc.* **2003**, *125*, 11761.

[13] a) Y. Kobori, S. Sekiguchi, K. Akiyama, S. Tero-Kubota, *J. Phys. Chem. A* **1999**, *103*, 5416; b) M. N. Paddon-Row, M. J. Shephard, *J. Phys. Chem. A* **2002**, *106*, 2935; c) M. Volk, T. Haberle, R. Feick, A. Ogrodnik, M. E. Michel-Beyerle, *J. Phys. Chem.* **1993**, *97*, 9831.

[14] a) Z. E. X. Dance, M. J. Ahrens, A. M. Vega, A. B. Ricks, D. W. McCamant, M. A. Ratner, M. R. Wasielewski, *J. Am. Chem. Soc.* **2008**, *130*, 830; b) J. Herbich, A. Kapturkiewicz, *Chem. Phys. Lett.* **1997**, *273*, 9.

[15] a) G. P. Wiederrecht, W. A. Svec, M. R. Wasielewski, T. Galili, H. Levanon, *J. Am. Chem. Soc.* **2000**, *122*, 9715; b) P. Ganesan, J. Baggerman, H. Zhang, E. J. R. Sudhoelter, H. Zuilhof, *J. Phys. Chem. A* **2007**, *111*, 6151.

[16] J. Langelaar, R. P. H. Rettschnick, G. J. Hoijtink, *J. Chem. Phys.* **1971**, *54*, 1.

[17] R. Livingston, D. W. Tanner, *Trans. Faraday Soc.* **1958**, *54*, 765.

[18] M. Banerjee, R. Shukla, R. Rathore, *J. Am. Chem. Soc.* **2009**, *131*, 1780.

[19] S. Samori, S. Tojo, M. Fujitsuka, S.-W. Yang, A. Elangovan, T.-I. Ho, T. Majima, *J. Org. Chem.* **2005**, *70*, 6661.

[20] a) H. Hayashi, *Introduction to Dynamic Spin Chemistry: Magnetic Field Effects upon Chemical and Biochemical Reactions*, World Scientific, Singapore, **2004**; b) U. E. Steiner, T. Ulrich, *Chem. Rev.* **1989**, *89*, 51.

[21] R. A. Marcus, *J. Chem. Phys.* **1965**, *43*, 679.

